

Generalized formula of moment gradient lateral torsional buckling factor for monosymmetric steel beams

Tarek Sharaf¹, Amr Reda^{2*}, Mohamed ElGhandour³, and Ashraf ElSabbagh⁴

¹ Associate Professor, Department of Civil Engineering, Port Said University, Egypt, email: tarek.sharaf@eng.psu.edu.eg

² Researcher, Department of Civil Engineering, Port Said University, Egypt, email: amrreda20152018@gmail.com

³ Associate Professor, Department of Civil Engineering, Port Said University, Egypt, email: dr.elghandor@gmail.com

⁴ Professor, Department of Civil Engineering, Port Said University, Egypt, email: ashraf_ims@yahoo.com

*Corresponding author, Email: amrreda20152018@gmail.com, DOI: 10.21608/psrj.2023.181357.1210

ABSTRACT

The lateral-torsional buckling (LTB) behavior of steel beams has been extensively reported. Most reports have been limited to study the doubly-symmetric beams besides a few other standard geometries. On the other hand, not so much research exists for monosymmetric steel beams, and LTB is one of the most critical design aspects for this type of beams. Codes allow the researchers to relate the critical moment to any in-plane loading to the standard uniform moment and members using the moment gradient factor. The moment gradient factor is an essential parameter in the design of steel cross-sections. Yet, it needs more to be applicable for cross-section shapes and boundary conditions. In this paper, a numerical model based on finite element analysis is presented, which is adopted to investigate the values of the moment gradient factor for different loading configurations. The model is developed to investigate the influence of load location with respect to the shear center of the beam section as well as the flange width ratio on the critical moment causing LTB. The numerical analysis results were validated, and new general equations for the moment gradient factor were developed to consider the effect of the different parameters.

Keywords: Steel Beams, Moment Gradient Factor, Monosymmetric Sections, Finite Element, Lateral Torsional Buckling.

Received 16-12-2022,

Revised 26-1-2023

Accepted 2-2-2023

© 2022 by Author(s) and PSERJ.

This is an open access article licensed under the terms of the Creative Commons Attribution International License (CC BY 4.0).

<http://creativecommons.org/licenses/by/4.0/>



1. INTRODUCTION

When elastic lateral-torsional buckling (LTB) occurs, structural stability is lost, and this is regarded as an ultimate limit state failure mode that must be considered when designing slender, long-span beams that are not supported laterally Bas [1]. LTB can also be described as the buckling of the compressed part of the beam when the vertically loaded beam rotates out of its plane due to bending. The critical load for the lateral-torsional buckling depends on the material properties, cross-sectional geometry, non-braced length, end restraint conditions, and type of loading. Furthermore, as presented by El-Mahdy and El-Saadawy [2], a 3D model has been created to study the LTB in I-beams that have a cross-sections with single axis of symmetry. They considered the influence of the span length of the beam

and the width of the flange of the cross-sections on the resistance results. They modeled the inelastic buckling behavior of the monosymmetric steel I-beam loaded by a uniform bending moment. Parametric studies have evaluated the moment gradient modification factor for stepped-shaped I-beams. In practice, most of the structural loads are not placed directly in the shear center of the cross-section but somewhat above or below it. The vertical position of the loading is essential only if the application point of the load is able to twist. When the load is placed above the shear center of the cross-section, the LTB capacity is smaller than in the case when loaded directly in the shear center. When the loads are applied below the shear center, the converse behavior takes place Kuś [3]. For flexural members having a non-uniform distribution of bending moments, it is possible to employ the equivalent uniform moment factor C_b , defined as C_1

in the Eurocode 3 Code [4], providing the ratio of the critical moments between a specific variable and uniform distribution of bending moments. The critical moment is defined as the bending moment causing the instability phenomenon; several researchers have worked on this topic. Dessouki et al. [5] considered three different loading positions: the top flange, the centroid of beam sections, and the bottom flange, to quantify the corresponding ultimate load capacities. The results showed that the lowest value of ultimate moment capacities was obtained when loads were applied at the top flange and the highest at the bottom flange. Anderson and Trahair [6] provided numerical solutions for beams with simply supported and cantilever boundary conditions and compared their predicted critical moments against experimental results. Kitipornchai and Trahair [7] proposed approximate expressions for the sectional properties required to determine critical moments for beams with I-sections having unequal flanges and lipped flanges. Lamb and Eamon [8] devised a method for generalizing a parametric solution that includes the effect of load position on the solution of the differential equation based on elastic stiffness. The expression proposed by Lamb and Eamon [8] was revised by Trahair [9]. Kitipornchai et al. [10] studied the buckling of monosymmetric I-section members stressed by linearly variable bending moments, including bending with either single curvature or reverse curvature. Extending the equations for the uniform bending moments to the behavior of monosymmetric T-beams exposed to variable bending moments has been discussed by Kitipornchai and Wang [11]. Several investigations on the LTB of monosymmetric cantilever T-beams have been carried out by Yuan et al. [12]. Lim et al. [13] studied the buckling of monosymmetric and doubly symmetric steel I-beams having end constraints and stressed by linearly variable bending moments. Serna et al. [14] investigated the LTB of symmetrical sections, with the load acting in the shear center. The paper offered a generic closed-form approach for computing the correction factor of variable moments for any moment distribution and end support conditions. Helwig et al. [15] Presented simplified C_b for simply supported monosymmetric I-girders with the loads applied at various positions of the cross-section. Park et al. [16] proposed a corrected moment modification factor for monosymmetric I-beams subjected to two kinds of loads, point loads and uniformly distributed loads, applied at various locations relative to the mid-height of the cross-section. Bresser et al. [17] proposed a solution in the form of a general formulation to determine equivalent moment factors for both I-sections and slender rectangular sections. It is noticed here that both papers only investigated the effect of lateral-torsional buckling of beams. However, torsional and flexural-torsional buckling effects are not investigated. For simply supported, doubly symmetric I-beams that are not allowed to deflect or twist but are able to spin laterally

and warping is possible, the critical moment, M_{ocr} , can be expressed as follows by Aydin et al. [18].

$$M_{ocr} = \frac{\pi}{L_b} \sqrt{E I_y G J} \sqrt{1 + W^2} \quad (1)$$

$$W = \frac{\pi}{L_b} \sqrt{\frac{E C_w}{G J}} \quad (2)$$

Where L_b is the laterally non-braced length equal to the span length; E stands for Young's modulus; G represents the shear modulus; I_y stands for the second moment of the area around the weak axis; J is the torsional constant; C_w is the warping constant, and W is the torsional slenderness parameter. If the moment distribution is not uniform, the critical value cannot be determined from Equation (1), and a modification is required. Most design codes include a solution for LTB of doubly symmetric I-member with unequal end moments in the form as follows:

$$M_{cr} = C_b M_{ocr} \quad (3)$$

where C_b is the moment gradient correction factor for taking into account the variable moment distribution within the non-braced length of the beam. For non-standard moment distributions, the AISC Specification AISC 360-16 [19] provides Equation (4),

$$C_b = \frac{12.5 M_{max}}{2.5 M_{max} + 3 M_A + 4 M_B + 3 M_C} \quad (4)$$

Where M_{max} Is the maximum absolute value of bending moments along L_b and M_A , M_B and M_C are the bending moments at points $L_b/4$, $L_b/2$ and $3 L_b/4$, respectively. On the other hand, The Canadian Steel Standard CAN-S16-14 [20] provides Equation (5)

$$C_b = \frac{4 M_{max}}{\sqrt{M_{max}^2 + 4 M_A^2 + 7 M_B^2 + 4 M_C^2}} \leq 2.5 \quad (5)$$

It is pointed out that the values of C_b in the current specifications ignore the end restraint conditions and the values of C_b are the same for every end constraint condition. According to the previous paragraph, the values of C_b are for doubly symmetric I-sections with loads applied at the mid-height of the section. The location of applied loads becomes essential when loads are not applied at mid-height. The buckling resistance of the beam is also affected by end restraint conditions.

The present study introduces a more accurate correction factor for the moment gradient factor for doubly symmetric, and monosymmetric I-beams loaded vertically at varying locations corresponding to the cross-section depth. The effects of loading position,

distribution of bending moments, and several end constraints are taken into account in the solution. The derivation of the elastic critical moment is carried out using finite element method.

2.DETAILS OF FINITE ELEMENT MODELS

In this section, finite element models are developed and validated against experimental results from the literature. The validated finite element models, which consider material and geometric nonlinearities and involve geometrical imperfections and residual stresses, are then used in the following sections to investigate the lateral torsional buckling of steel I-beams.

The numerical model used in this article is validated against the experiments presented in previous research by Yang et al. [21] and Surla and Park [22], where further details can be found. In summary, the general models' characteristics are presented below:

2.1. Finite element modeling and material

The nonlinear computations were performed using the commercial finite element software ABAQUS [23]. It can consider geometric and material non-linearities in the given model. Large displacement effects were accounted for by utilizing the nonlinear geometry option in [23]. Four-node shell elements with reduced integration S4R were used for steel beams, as suggested by Bradford and Liu [24], which can avoid shear and membrane locking. This element can be used to consider membrane strain and transverse shear deformation. Each of the four nodes has six DOFs, 3 translational and 3 rotational.

Figure (1) shows the constitutive models for 8 mm and 16 mm thick steel plates [21]. A tri-linear kinematic hardening model with von Mises yield criterion was used for 8 mm steel plate in the beam web and bottom flange. As for 16 mm steel plate in the top flange, a multi-linear stress-strain relationship was defined to take account of the yield plateau. Parameters in the mode were determined from coupon tests on steel plates. The yield strengths of the 8 and 16 mm plates were 530 and 481 MPa, respectively, and the corresponding modulus of elasticity were 209 and 204 [21]. However, only engineering stress and strain were obtained in the coupon tests. In the numerical model, true stress and strain were incorporated instead of engineering stress and strain, as expressed in Equations (6) and (7).

$$\sigma_{true} = \sigma_{nom}(1 + \varepsilon_{nom}) \quad (6)$$

$$\varepsilon_{true} = \ln(1 + \varepsilon_{nom}) - \frac{\sigma_{true}}{E} \quad (7)$$

Where σ_{true} and ε_{true} are true stress and strain, σ_{nom} and ε_{nom} are engineering stress and strain.

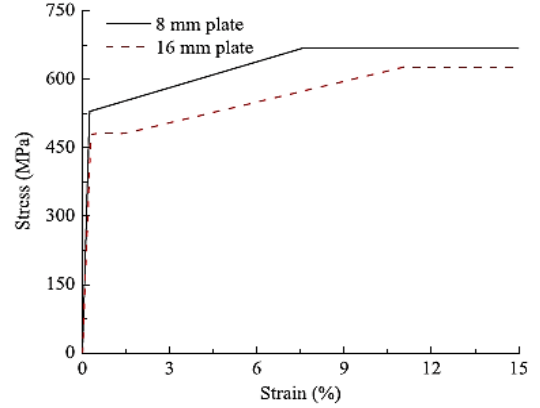


Figure 1: Stress-strain relationship [21].

2.2. Residual stress and initial geometric imperfections

The residual stresses were applied to the FEA models using the *INITIAL CONDITION command in the FE program. Figure (2) show the distribution of longitudinal residual stress, measured on steel beams using the sectioning method, and the measured values of each section were used in the FEA models Yang et al. [25]. By partitioning the web and flanges of the cross-section, residual stresses were introduced into the FEA models. The current study did not consider geometric imperfections as the used cross-sections range between compact and non-compact cross-sections. Thus, the effect of initial geometric imperfections could be minor. Although Yang et al. [21] has considered the effect of imperfection, but the present results without imperfections show very good agreement with the experimental results.

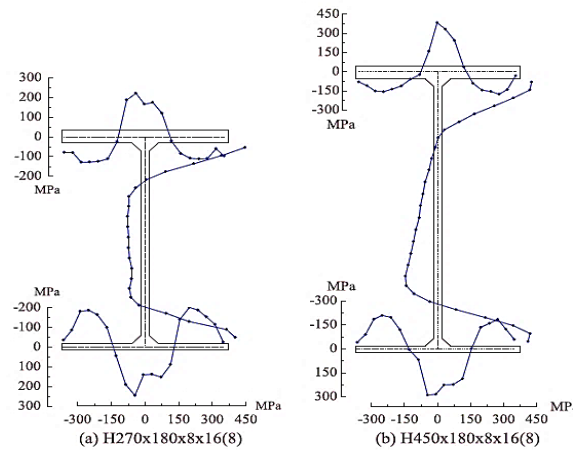


Figure 2: Residual stress distribution of I-sections [25].

2.3. Loads and Boundary conditions

Figure (3) shows a steel plate of 25×50 mm was used in introducing the vertical point load at the mid-span of the beam [21]. The load was applied in increments as static point load using the RIKS method available in [23] library. In this way, it is possible to obtain load proportionality factors and their respective increments associated with the model's nodal displacement data, allowing tracing of the load–displacement curves. With these curves, it is then possible to obtain the ultimate load of the model.

To simulate the boundary conditions in the experimental [21], lateral restraints were applied to the top and bottom flanges at the midspan and two ends of the beams. Simple vertical supports were considered at both ends of the beam, Figure (4).

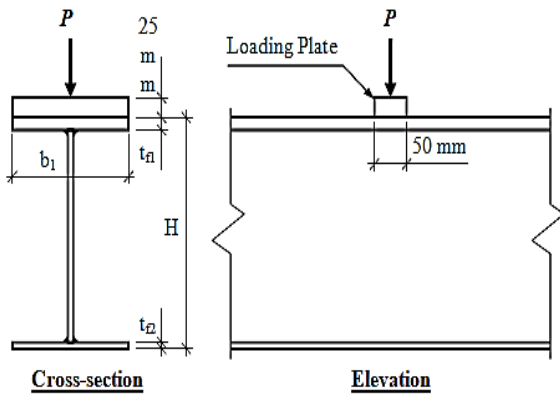


Figure 3: Dimensions of tested cross-sections and dimensions of loading plate used in FE simulation [21].

2.4. Validation of finite element models

In this section, the accuracy of the finite element model of the steel beams is investigated. The comparison was performed using the available results of a test program on the LTB behavior of steel beams, according to [21]. In the test program, six singly symmetric Q460GJ steel beams were subjected to concentrated point loads during testing [21]. The dimensions and details of specimens are displayed in Figure (3) and summarized in Table 1.

The compressed top flange of the beam was reinforced with an additional plate of 16 mm thickness, while the thickness of the web and bottom flange was 8 mm. Two types of I-sections were used for the beams. The height-to-width ratios of the cross-sections were around 1.5 and 2.5 to prevent local buckling in the beam web. Transverse stiffeners of 8 mm thickness were applied at the loaded section and end supports to prevent the web from being crippled. The test arrangement of the specimens [21] is presented in Figure (4).

Table 1. Specimens details [21].

Specimen	L (m)	H (mm)	tw (mm)	tfl (mm)	b1 (mm)	t2 (mm)
D-6-1.5	6	269.26	8.39	16.72	179.30	8.16
D-7-1.5	7	270.56	8.97	16.67	178.86	8.20
D-8-1.5	8	270.82	8.39	16.90	179.23	8.29
D-6-2.5	6	449.66	8.82	16.60	179.99	8.43
D-7-2.5	7	450.95	8.59	16.27	180.93	8.59
D-8-2.5	8	450.54	8.83	16.81	179.39	8.54



Figure 4: Test specimen and loading arrangement [21].

The other verification is done on the experimental work by [22]. The dimensions and details of the tested specimens are displayed in Figure (5) and summarized in Table 2.

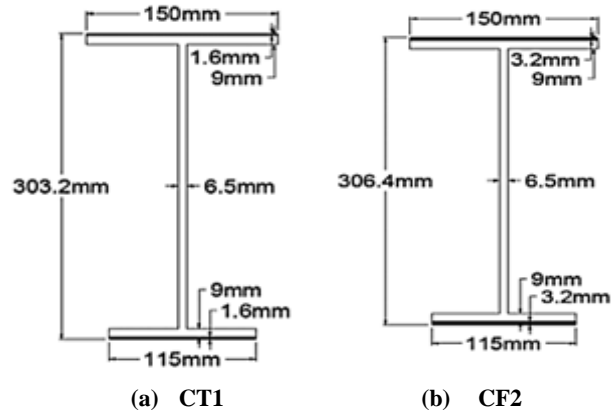


Figure 5: Dimensions of tested cross-sections [22].

Three meshes, coarse, intermediate, and fine, were built for the specimen D-8-1.5 and the total number of elements in these was 10968, 37592, and 119540, as shown in Figure (6). This is to explore the effect of mesh size on the FE solution's accuracy and processing time. The current FE model was verified against experimental and FEA findings by [21] and [22].

Table 2. Specimens details [22].

Specimen	L (m)	H (mm)	t _w (mm)	t _{fl} (mm)	b ₁ (mm)	t ₂ (mm)
CT1	3	303.2	6.5	9	150	115
CF2	4	306.4	6.5	9	150	115

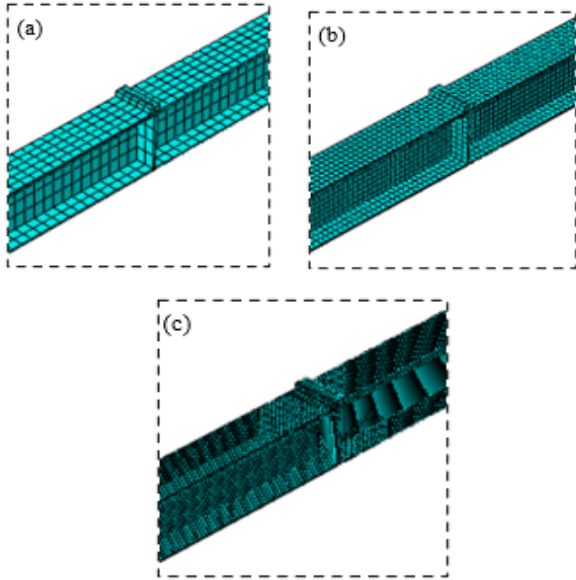


Figure 6: a) coarse mesh, b) intermediate mesh, and c) fine mesh.

Figures (7) and Figure (8) show the present FE analyses and test results comparisons. Accordingly, the fine mesh models provided the most precise agreement, but the processing times are the longest and require the maximum space on the computer. The findings using the coarse meshing were not as accurate but required least time and storage space when processing. Finally, the effects achieved with intermediate mesh are comparable to those achieved with fine mesh. Due to these factors, the accuracy, processing time, and storage capacity for the finite element analyses is most profitable using the intermediate mesh size.

Figure (9) presents the failure mode of beam D-8-1.5 obtained using this FE model and the experimental work [21]. The FEA failure modes are compared with its

experimental failure modes, and it is found that the FEA failure modes are in good agreement with the experimental failure modes.

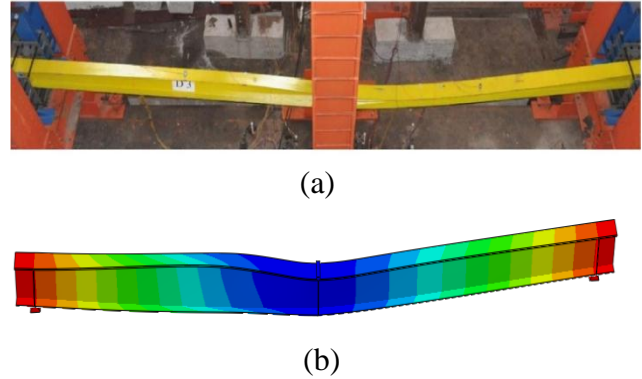


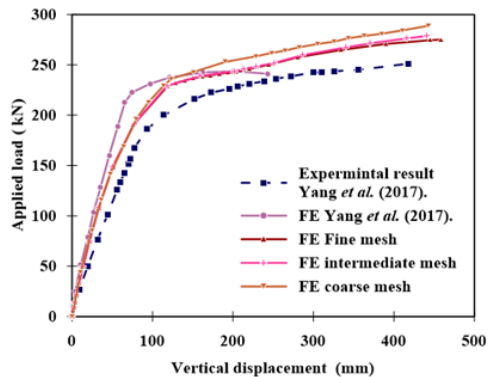
Figure 9: Mode of failure in the tested beam[21] and the respective FEA model; a) Experimental failure, FE model failure, and b) The failure mode of beam D-8-1.5.

Comparisons are done between the experimental and numerical load capacities of steel beams, as shown in Table 3. The numerical results have a mean FE / experimental load ratio of 0.98, indicating good agreement.

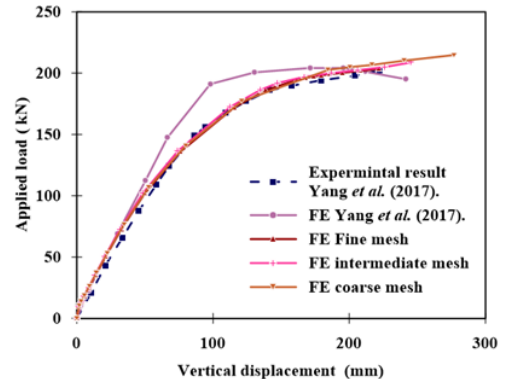
Consequently, the numerical model can make precise predictions regarding the buckling load of steel beams.

Table 3. Comparison of buckling loads for model validation from experiments[21]

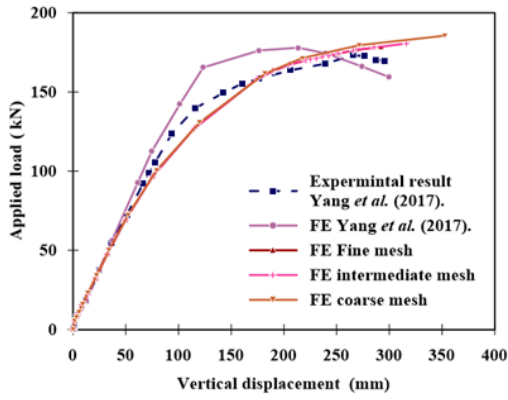
Specimen	FE analysis	Experiment	P _{FE} /P _{Exp}	Δ error %
	P _{FE} (kN)	P _{Exp} (kN)		
D-6-1.5	245.22	252.9	0.97	3.04
D-7-1.5	200.28	201.2	1.00	0.46
D-8-1.5	174.74	171.8	1.02	1.71
D-6-2.5	469.36	492.5	0.95	4.70
D-7-2.5	365.11	378.2	0.97	3.46
D-8-2.5	315.51	319.4	0.99	1.22
Mean Value			0.98	

$$\Delta = (P_{Exp} - P_{FE}) / P_{Exp} \times 100$$


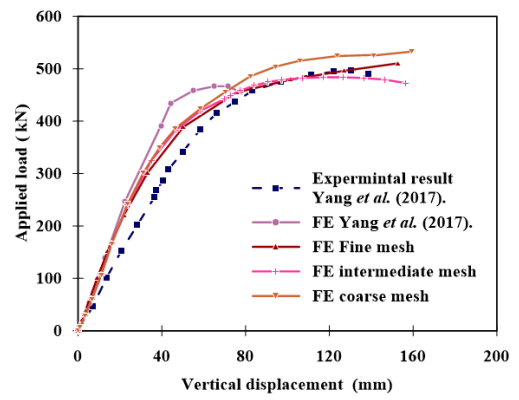
(a) D-6-1.5



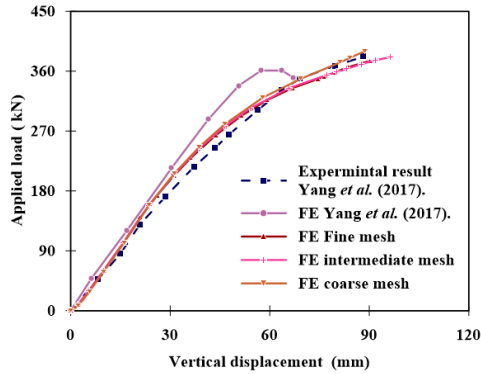
(b) D-7-1.5



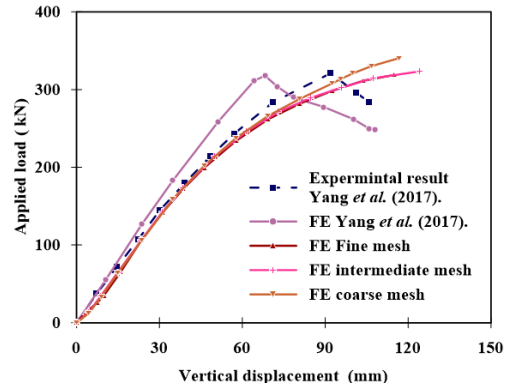
(C) D-8-1.5



(d) D-6-2.5

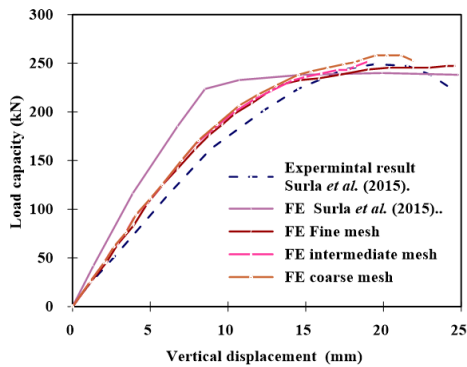


(e) D-7-2.5

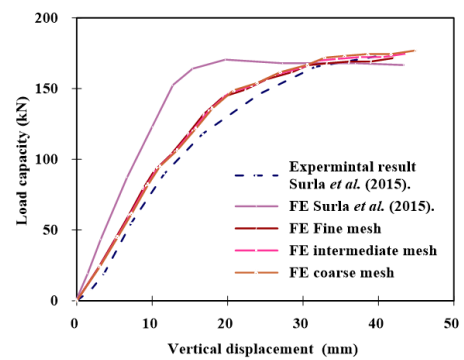


(f) D-8-2.5

Figure 7: Load–deflection curves for experiments [21] and finite element.



(a) CT1



(b) CF2

Figure 8: Load–deflection curves for experiments [22] and finite element.

3.PARAMETRIC STUDY

A total of 1700 3D FE models of steel I-beams were created and analyzed to determine the critical moment's values. The studied parameters included the depth of the beam section, 300, 400, 500, and 600 mm; the span length of the beam, 4000, 6000, 8000, and 12000 mm. The thickness of the top and bottom flanges 10, 13, 16, and 19 mm, and the variation of the flange widths as

listed in Table 4. Also, the loading type, position on the vertical axis of the cross-section and type of end supports are investigated. The types of loading investigated in this study are the end moments in the span, point load at the mid-span, and uniformly distributed load in the span of loading. The loads were applied to the top of the beam, shear center, and bottom flange. The end restraints considered are simple supports and fully fixed ones.

Table 4. Cross-section dimensions of the models included in the parametric study.

Designation	Section height H (mm)	Web thickness t_w (mm)	Top flange width b_1 (mm)	Bottom flange width b_2 (mm)	Top and bottom flange thickness t_f (mm)	$\beta_f = b_1/b_2$
I300A	300	7	150	300	10	0.5
I400A	400	8	180	360	13	0.5
I500A	500	11	200	400	16	0.5
I300B	300	7	150	225	10	0.67
I400B	400	8	180	270	13	0.67
I500B	500	7	200	300	16	0.67
I300C	300	7	150	150	10	1
I400C	400	8	180	180	13	1
I500C	500	11	200	200	16	1
I300D	300	7	225	150	10	1.5
I400D	400	8	270	180	13	1.5
I500D	500	7	300	200	16	1.5
I300E	300	7	300	150	10	2
I400E	400	8	360	180	13	2
I500E	500	7	400	200	16	2

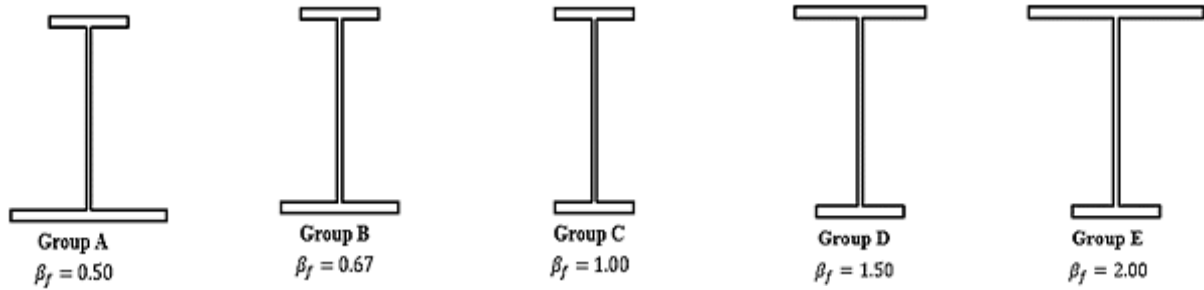


Fig 10: Different section groups.

All these parameters are incorporated in determining the moment-gradient factor, C_b . The models were divided into five groups, A, B, C, D, and E, on account of the value of the width ratio $\beta_f = b_1/b_2$. All groups except C with doubly symmetric cross-sections contain monosymmetric cross-sections, as presented in Figure (10).

The yield strength of steel is 500 MPa, the corresponding modulus of elasticity was 210 GPa, the shear modulus of elasticity $G = E/2(1 + \nu)$, and Poisson's ratio $\nu = 0.3$. In addition, the residual stress distributions are considered similar to [21].

Figure (11) presents the beams' cross-sectional details and the loads' vertical locations.

The intermediate mesh size was selected as described in the exploratory FE studies.

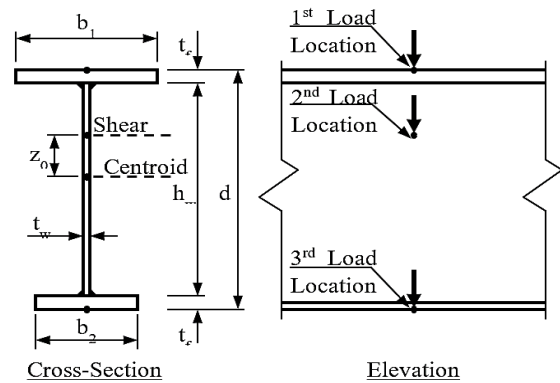


Fig 11: Details of the cross-section and load locations.

Boundary conditions adopted for this study are shown in Figure (12). In this Figure, the longitudinal beam direction is denoted (1), while the direction (2) represents the vertical axis, and the direction (3) passes through the major axis of the beam's cross-section.

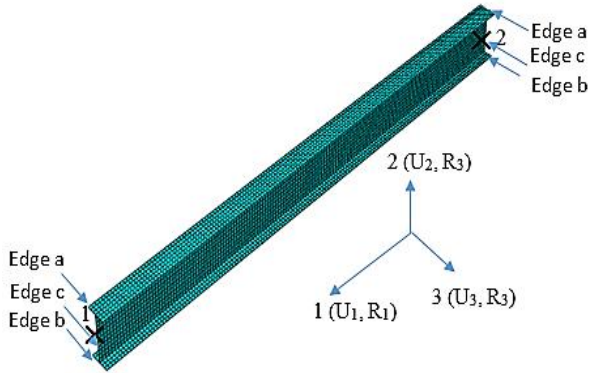


Figure 12: FE mesh and boundary conditions.

- a) The beam end (1) is hinged support:
 - The displacements in directions (1, 2, and 3) are restrained, as well as the rotation around direction (1).
 - The edges a, b, and c are restricted in direction 3. The displacement of edge (b) in direction (1) is restrained.
- b) The beam end (2) is roller support:
 - The displacement in directions (2 and 3) and the rotation in direction (1) are restrained.
 - The edges a, b, and c are restricted from out-of-plane movement (direction 3).

4.RESULTS AND DISCUSSIONS

The results of simply supported beams point-loaded at different vertical locations at the mid-span are discussed first. The span length of the beam and widths of top and bottom flanges in each cross-section were varied when calculating the critical buckling loads, Table (5) shows the factors for steel I300 beams of span 6000 mm subjected to mid-span point loads, uniformly

distributed load, and equal end moments. The elastic critical uniform moment, M_{ocr} , is calculated using Eq. (1). Figure (13) shows the typical failure mode of a steel beam under a concentrated point load and the obtained values of M_{cr} of the buckling moment is calculated from the value P_{cr} of the buckling load evaluated once the FE solution came to singularity (divergence) that detects the buckling load for a given beam.

$$M_{cr} = \frac{P_{cr} L}{4} \quad (8)$$

The results are presented in Figure (14), showing the relation between C_b and span length L , as well as the design value of C_b in EC3. The factor is not constant throughout the beams' complete range of slenderness values, although EC3 provides only a constant value of 1.35 independent of the slenderness. The difference between the factors computed using the nonlinear FEM and the one given by EC3 decreases with the increase of the non-braced length. In groups A, B, and C, factor C_b has the most significant values when the load is located at the bottom flange. When the load location is moved towards the upper flange, the value of C_b decreases. When the load is at the bottom flange in groups D and E, the values of C_b are smaller than the ones for other locations of load.

Selcuk [26] introduced a non-dimensional slenderness ratio λ_{LT} shown as Equation (9), valid independent of the beam's span length and cross-section properties.

$$\lambda_{LT} = \sqrt{\frac{M_p}{M_{ocr}}} \quad (9)$$

where $M_p = F_y Z_p$ is the plastic bending resistance of the cross-section and Z_p is its plastic modulus. Equation (10), includes a factor M_f for modifying the value of C_b in EC3 based on the FEM results. The values presented in Table 5 are for beams subjected to mid-span point loads, uniformly distributed load, and equal end moments considered in the parametric study. The values are also plotted in Figure (15).

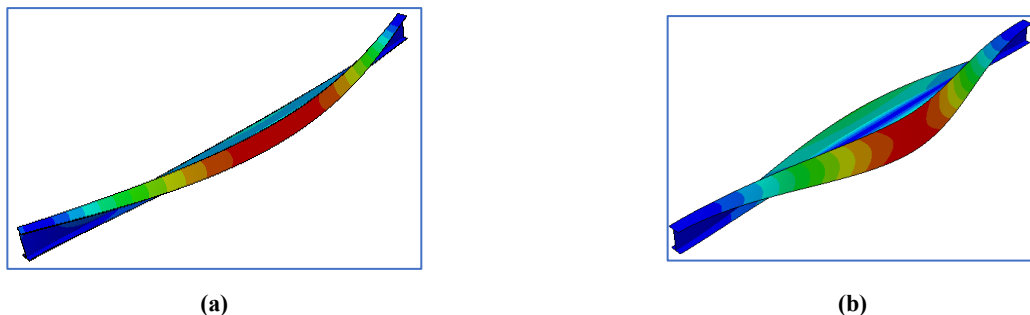


Figure 13: The failure mode of beam I300A with 6000 mm span in the FEM.; a) Simple support beam, and b) Fixed end

Table 5: Factors for simply supported steel I300 beams with 6.0m span.

Model	$M_{ocr}, kN.m$	$M_{cr} (FEM), kN.m$			$C_b (FEM)$			λ_{LT}	M_f		
		Top flange	Shear center	Bot flange	Top flange	Shear center	Bot flange		Top flange	Shear center	Bot flange
a) Factors subjected to mid-span point load.											
I300AL6	251.431	84.509	199.314	240.029	0.336	0.793	0.955	1.246	0.249	0.587	0.707
I300BL6	137.493	77.814	146.369	195.567	0.566	1.065	1.422	1.626	0.419	0.789	1.054
I300CL6	74.643	71.190	99.903	110.060	0.954	1.338	1.474	2.053	0.706	0.991	1.092
I300DL6	137.493	168.444	194.942	120.045	1.225	1.418	0.873	1.626	0.907	1.050	0.647
I300EL6	251.431	298.335	273.869	128.310	1.187	1.089	0.510	1.246	0.879	0.807	0.378
b) Factors subjected to a full span uniform distribution load.											
I300AL6	251.43	76.37	156.02	177.69	0.30	0.62	0.71	1.25	0.27	0.55	0.63
I300BL6	137.49	69.71	120.46	148.86	0.51	0.88	1.08	1.63	0.45	0.78	0.96
I300CL6	74.64	63.20	85.89	103.27	0.85	1.15	1.38	2.05	0.75	1.02	1.22
I300DL6	137.49	150.23	173.47	112.16	1.09	1.26	0.82	1.63	0.97	1.12	0.72
I300EL6	251.43	228.28	215.44	120.23	0.91	0.86	0.48	1.25	0.80	0.76	0.42
c) Factors subjected to equal end moments.											
I300AL6	251.43		101.56			0.40		0.40		1.25	
I300BL6	137.49		89.62			0.65		0.65		1.63	
I300CL6	74.64		77.44			1.04		1.04		2.05	
I300DL6	137.49		138.23			1.01		1.01		1.63	
I300EL6	251.43		152.66			0.61		0.61		1.25	

$$M_f = \frac{C_b (FEM)}{C_b (Code)} \quad (10)$$

$$C_b (FEM) = \frac{M_{cr} (FEM)}{M_{ocr}} \quad (11)$$

The value of $C_b (FEM)$ will be named here after \bar{C}_b for design purposes and can be obtained as

$$\bar{C}_b = C_{b(code)} \times M_f \quad (12)$$

The values for the modification factor M_f are computed using Equation (1) and listed in Table 5. Figure (10) shows the relationship between λ_{LT} and M_f . The curves nearly coincide for each group A, B, C, D, and E, location of the load and cross-section.

Therefore, the proposed equations are based on the polynomial curve best fitting of the modification factor M_f extracted from FE analysis.

To represent M_f for any cross-section in each group, and location of the load can be expressed as:

$$M_f = a \lambda_{LT}^3 + b \lambda_{LT}^2 + c \lambda_{LT} + d \quad (13)$$

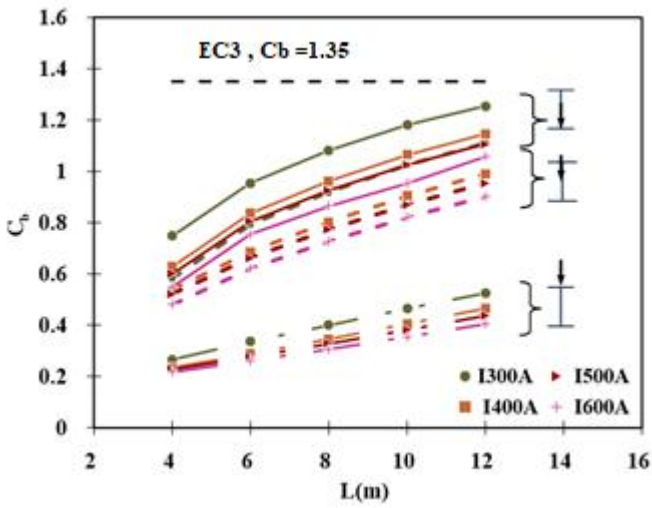
The parameters a, b, c, and d are presented in a general formula as in Equation (14),

$$x = \alpha_{x4}\beta_f^4 + \alpha_{x3}\beta_f^3 + \alpha_{x2}\beta_f^2 + \alpha_{x1}\beta_f + \alpha_{x0} \quad (14)$$

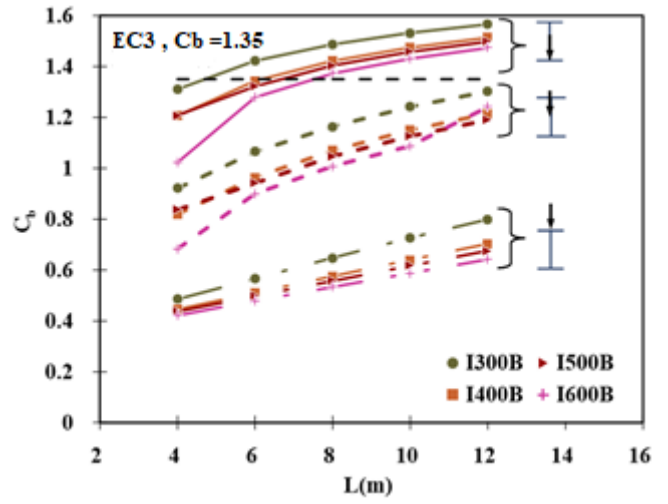
Where x represents any of the parameters a, b, c, or d, as shown in Table 6.

The factor β_f can also represent the ratio between areas of the compressive and tensile flanges since the thickness of both flanges is equal, as shown in Table 5.

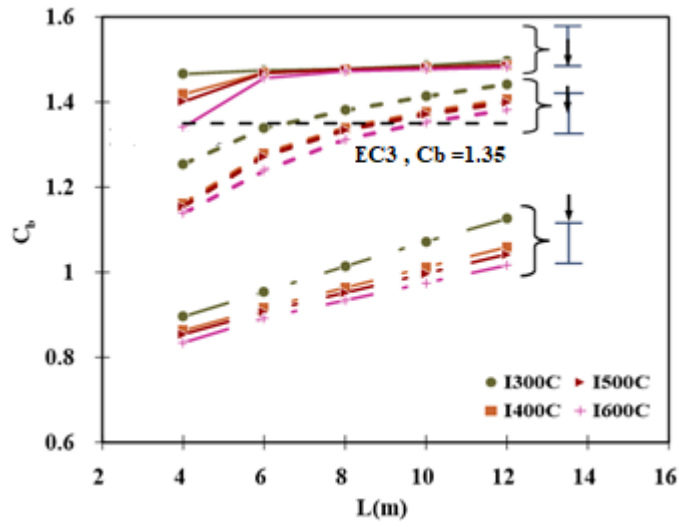
Similarly, the relationship between M_f and λ_{LT} for the simply supported and uniformly loaded beam is shown in Figure (16). Again, it is seen that for each group A, B, C, D, and E, cross-section and location of the load, the curves almost coincide. Figure (17) shows that the same conclusion is valid for a simply supported beam with a uniform moment along the span. Thereby, similar expressions for M_f were deduced and are listed in Table 6.



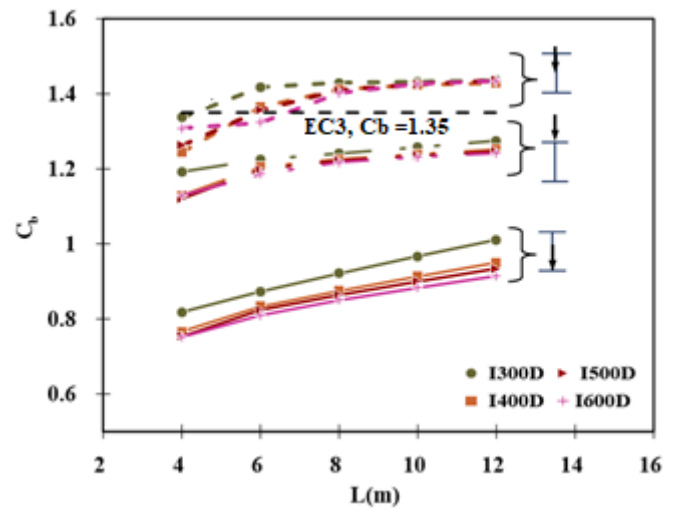
(a)



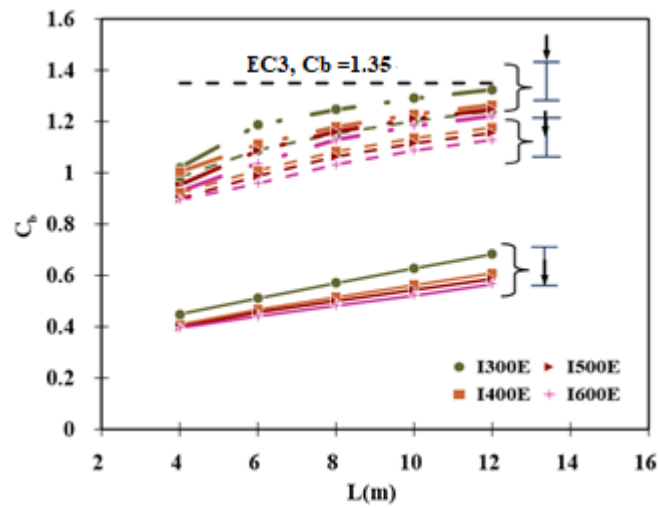
(b)



(c)

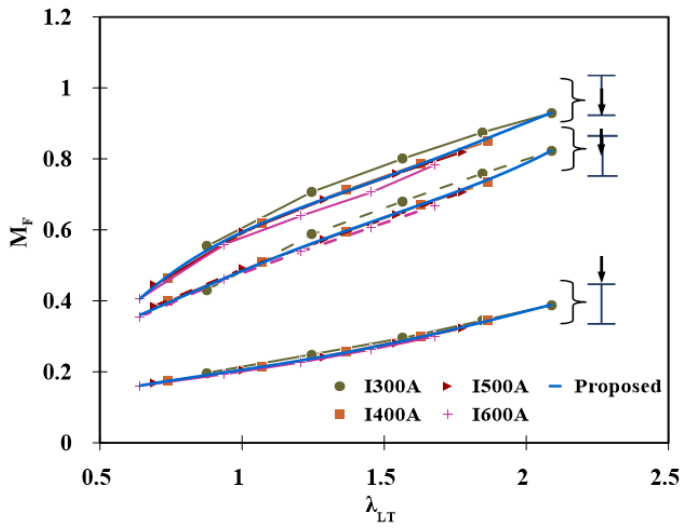


(d)

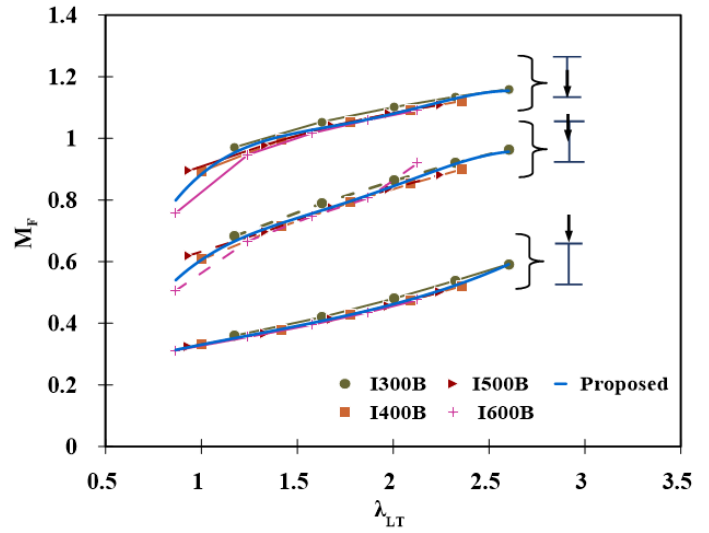


(e)

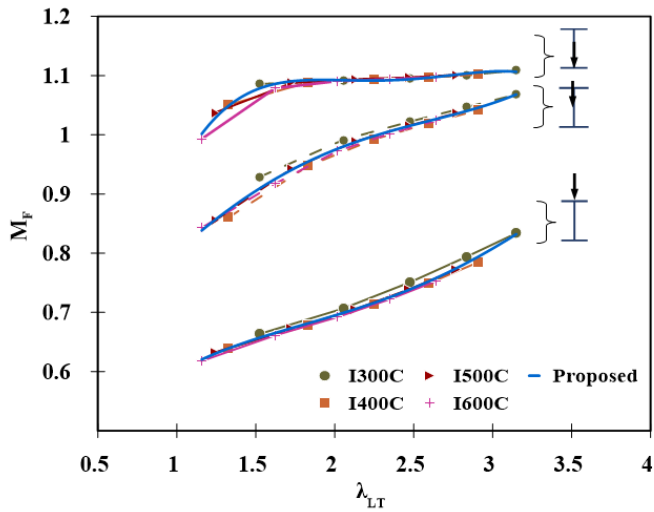
Figure 14: C_b - L diagrams for model beams subjected to point loading at mid-span; a) Group A, b) Group B, c) Group C, d) Group D, and e) Group E.



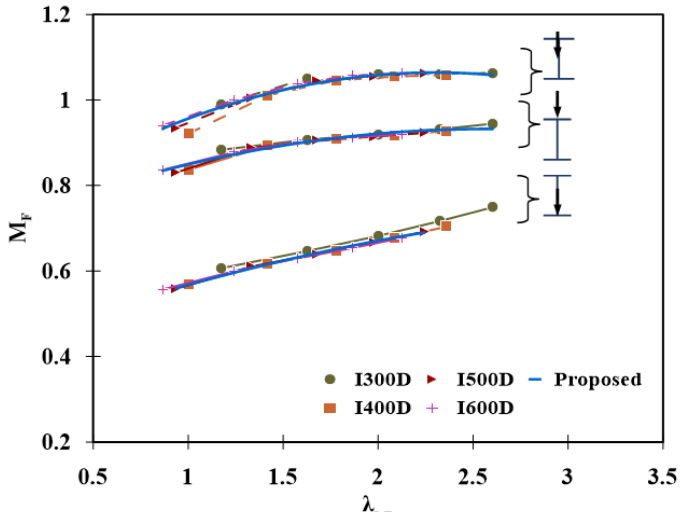
(a)



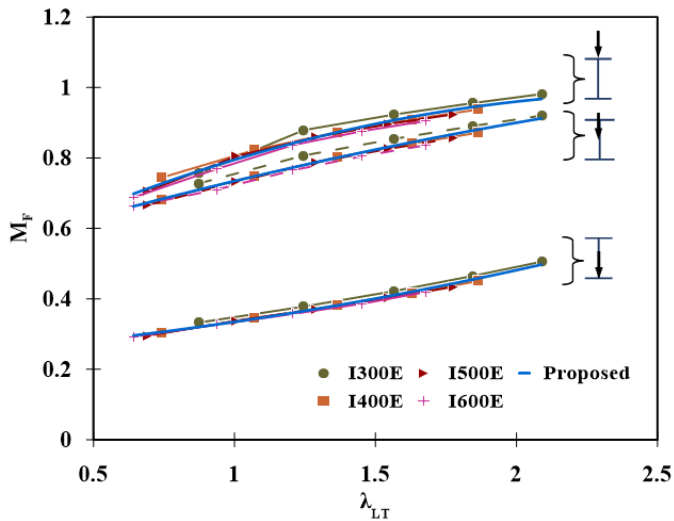
(b)



(c)

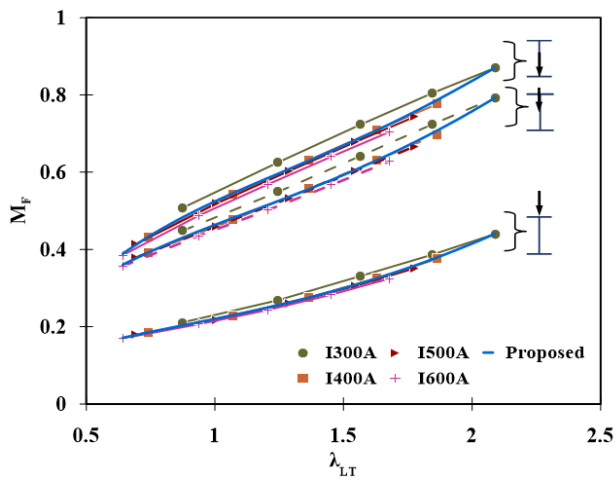


(d)

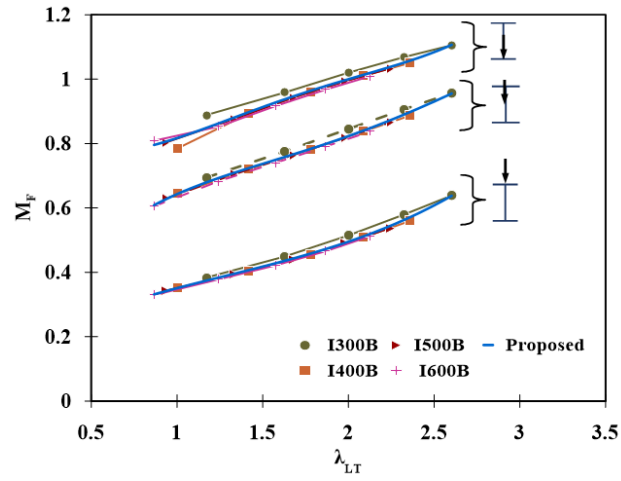


(e)

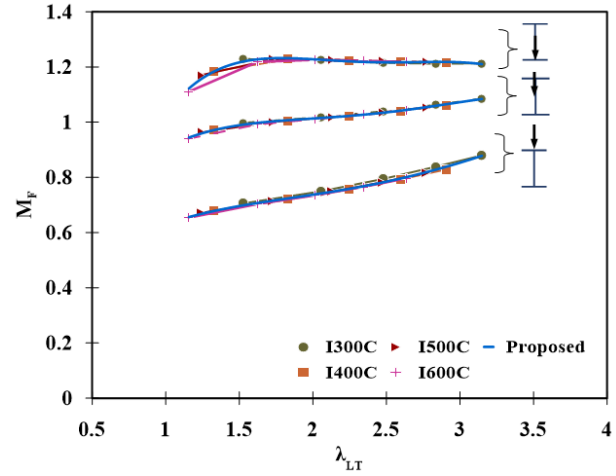
Figure 15: M_F - λ_{LT} diagrams for model beams subjected to point loading at mid-span; a) Group A, b) Group B, c) Group C, d) Group D, and e) Group E.



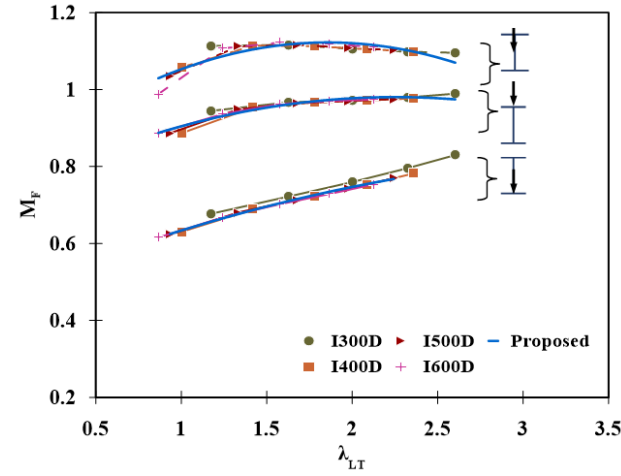
(a)



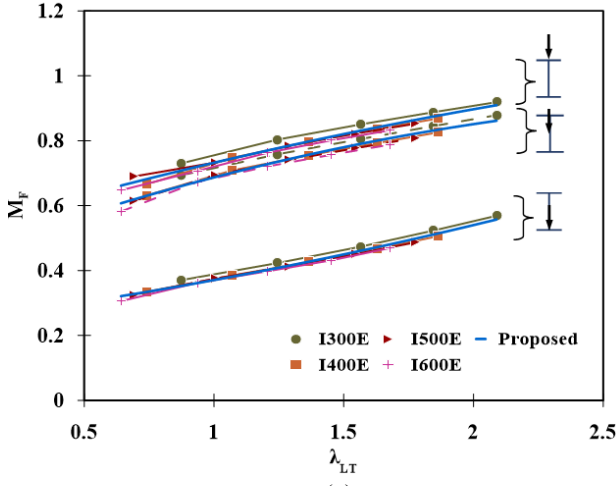
(b)



(c)

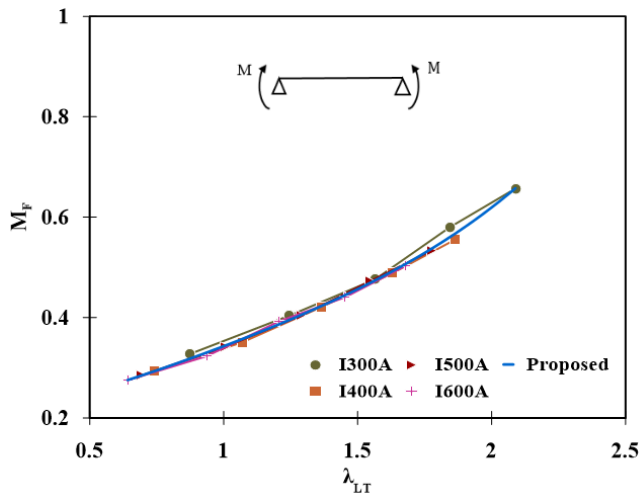


(d)

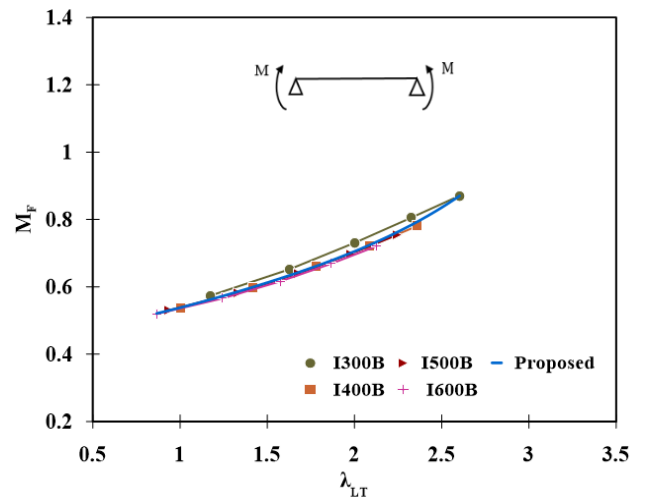


(e)

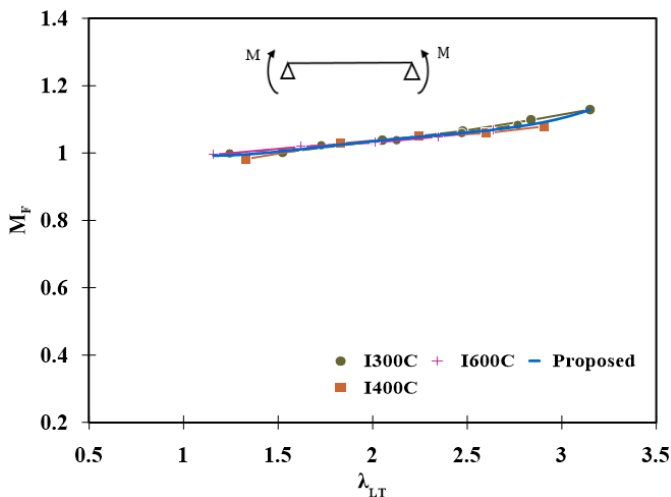
Figure 16: M_F - λ_{LT} diagrams for model beams subjected to a uniformly distributed load; a) Group A, b) Group B, c) Group C, d) Group D, and e) Group E.



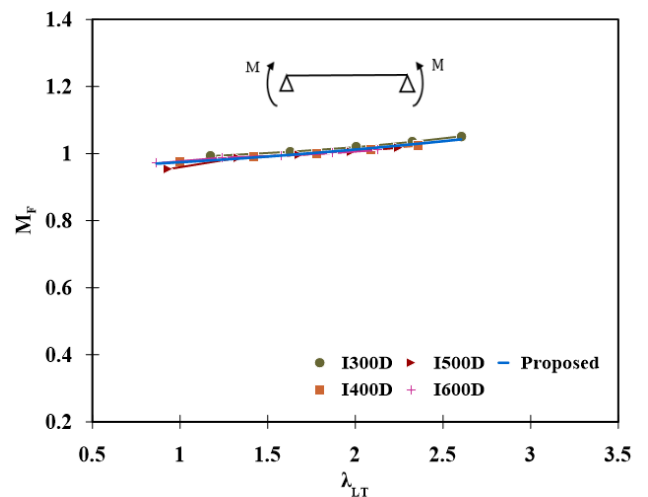
(a)



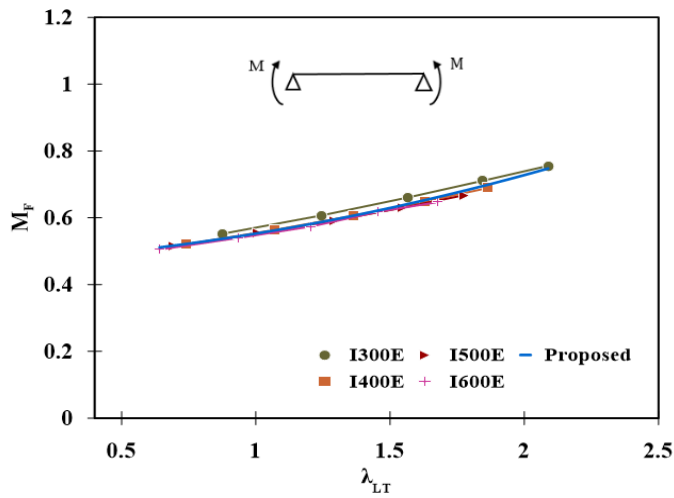
(b)



(c)



(d)



(e)

Figure 17: M_F - λ_{LT} diagrams for model beams subjected to equal end moments; a) Group A, b) Group B, c) Group C, d) Group D, and e) Group E.

Table 6: (a) Coefficients for modification factor M_f for simply supported beams.

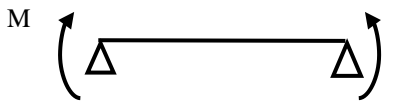
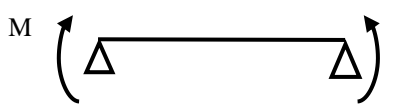
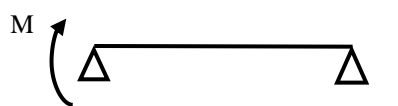
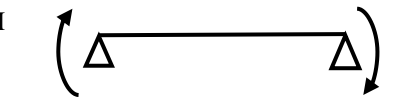
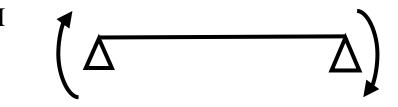
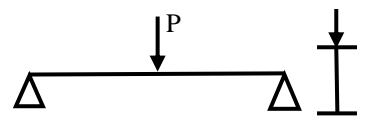
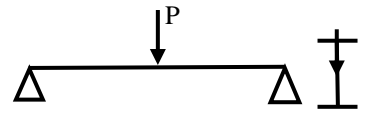
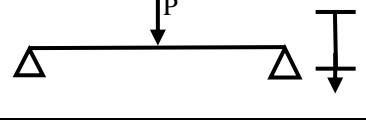
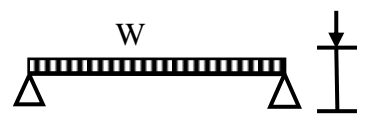
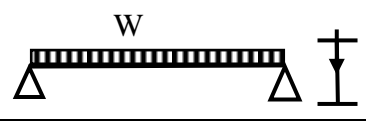
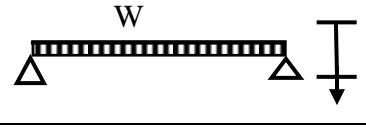
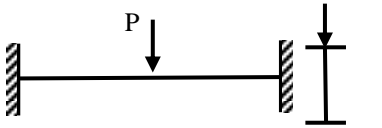
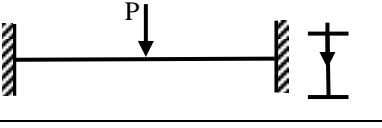

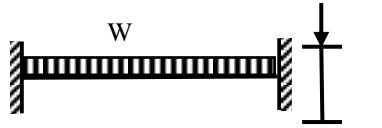
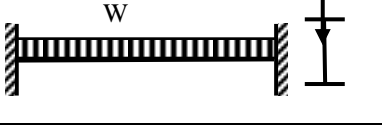
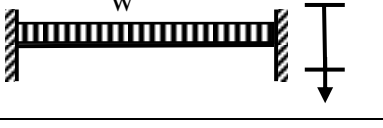
Loading	C_b EC3	x	α_{x4}	α_{x3}	α_{x2}	α_{x1}	α_{x0}
(a) Beams subjected to end moments.							
	1.0	a	0.0	0.0	0.0	0.0	0.0
		b	0.016	-0.11	0.30	-0.39	0.19
		c	0.02	-0.04	0.13	-0.28	0.18
		d	1.59	-7.66	11.57	-5.43	0.88
	1.30	a	0.0	0.0	0.0	0.0	0.0
		b	0.06	-0.33	0.68	-0.66	0.27
		c	-0.13	0.73	-1.28	0.75	-0.08
		d	1.24	-6.32	9.94	-4.67	0.77
	1.75	a	0.0	0.0	0.0	0.0	0.0
		b	0.38	-1.84	2.86	-1.84	0.47
		c	-1.77	8.27	-12.30	7.09	-1.28
		d	2.34	-11.64	18.25	-9.78	1.84
	2.3	a	0.0	0.0	0.0	0.0	0.0
		b	1.46	-6.55	9.72	-5.90	1.25
		c	-5.85	25.96	-38.04	22.59	-4.47
		d	5.59	-25.05	36.56	-20.21	3.92
	2.3	a	0.0	0.0	0.0	0.0	0.0
		b	0.65	-3.06	4.86	-3.06	0.56
		c	-3.35	15.79	-25.41	16.29	-3.10
		d	4.44	-20.31	30.68	-17.28	3.32
(b) Beams subjected to point load at mid-span.							
	1.35	a	0.0	0.0	0.0	0.0	0.0
		b	0.24	-1.09	1.67	-1.11	0.30
		c	-0.86	3.89	-5.82	3.50	-0.68
		d	1.11	-5.34	8.29	-4.26	0.77
	1.35	a	0.0	0.0	0.0	0.0	0.0
		b	0.26	-1.15	1.74	-1.05	0.19
		c	-0.97	4.39	-6.50	3.50	-0.23
		d	0.68	-3.08	4.04	-0.80	-0.13
	1.35	a	0.0	0.0	0.0	0.0	0.0
		b	-0.22	1.27	-2.67	2.45	-0.83
		c	0.06	-1.31	5.03	-6.69	2.90
		d	0.18	1.63	-9.21	12.7	4.21
(c) Beams subjected to uniformly distributed load along the span.							
	1.13	a	0.0	0.0	0.0	0.0	0.0
		b	0.09	-0.45	0.77	-0.60	0.20
		c	-0.39	2.03	-3.49	2.34	-0.48
		d	0.51	-2.96	5.19	-2.51	0.42
	1.13	a	0.0	0.0	0.0	0.0	0.0
		b	0.60	-2.70	4.17	-2.66	0.60
		c	-2.26	10.17	-15.27	8.87	-1.51
		d	2.01	-9.23	13.26	-5.99	0.92
	1.13	a	0.0	0.0	0.0	0.0	0.0
		b	-0.06	0.37	-0.76	0.68	-0.22
		c	-0.57	2.07	-1.62	-0.95	1.04
		d	2.96	-11.93	13.71	-3.04	-0.44

Table 6: (b) Coefficients for modification factor M_f for fixed end supports.

Loading	C_b EC3	x	α_{x4}	α_{x3}	α_{x2}	α_{x1}	α_{x0}
(a) Beams subjected to point load at mid-span.							
	1.68	a	-1.57	7.65	-12.25	7.64	-1.24
		b	9.84	-48.22	80.06	-54.24	10.90
		c	-16.69	81.89	-138.89	99.34	-21.85
		d	7.89	-38.49	65.76	-48.43	11.33
	1.68	a	2.75	-15.55	30.70	-24.82	7.04
		b	-11.92	67.29	-132.85	107.29	-30.89
		c	17.36	-96.69	188.17	-149.25	43.76
		d	-10.30	54.70	-101.27	76.13	-21.10
	1.68	a	-16.95	85.05	-150.09	109.17	-26.96
		b	79.84	-400.15	704.66	-510.35	124.35
		c	-122.71	615.28	-1083.90	783.71	-188.6
		d	59.85	-300.60	530.57	-384.11	92.34
(b) Beams subjected to uniformly distributed load along the span.							
	2.58	a	-0.14	0.21	0.59	-0.98	0.53
		b	0.84	-1.77	-0.68	1.30	-1.25
		c	0.51	-6.13	14.36	-7.42	2.30
		d	-2.30	13.22	-24.30	14.90	-3.3
	2.58	a	-3.92	18.92	-32.01	22.15	-4.68
		b	22.62	-110.77	191.31	-136.43	29.85
		c	-40.14	199.54	-352.68	259.79	-58.49
		d	21.50	-108.02	193.89	-145.76	34.24
	2.58	a	-1.80	9.14	-15.96	11.06	-2.22
		b	11.41	-58.24	103.70	-73.98	15.564
		c	-21.99	113.79	-206.65	151.15	-32.68
		d	12.02	-63.05	116.51	-87.20	19.96

5. SUMMARY AND CONCLUSIONS

The current research focuses on analyzing the elements that impact the value of the factor of moment-gradient of both doubly symmetric and monosymmetric steel beams. Steel beams of both doubly symmetric and monosymmetric configurations are the subject of this study, which examines the variables that influence the moment-gradient factor. Three-dimensional beam models were used to conduct this investigation. An intensive parametric study was carried out using 1700 3D-FE models of steel I-beams. These models have been analyzed under three distinct loading scenarios for different beam lengths; variable end moments, concentrated load in the middle of the span, and an evenly distributed load. Three load locations were applied to the cross-section at distinct heights. Non-dimensional modified flexural-torsional slenderness of the beam was computed for each span length and incorporated geometric features of the beam and its

cross-section to generalize the findings. A moment-gradient modification factor was also developed as a

function of the different parameters to quantify the variance in outcomes. The results of the FEA verification and parametric studies show that. For each span length, the factor of moment-gradient was calculated, and in order to generalize the results, geometric details of the beam and its cross-section were included in the non-dimensional modified flexural-torsional slenderness of the beam $\lambda_{L,T}$. Furthermore, to quantify the variation of results based on $\lambda_{L,T}$, moment-gradient modification factor M_f was introduced as a function of $\lambda_{L,T}$. The results of the FE analyses and the parametric studies show that:

1. The factor of moment-gradient C_b is not only dependent on the condition of loading but also the beam span length and beam slenderness. Shorter spans generally have lower C_b value, which rises with increasing span length.

2. When the compression flange has an area less than or equal to the area of the tension flange, the value of the C_b decreases when the load location changes from the bottom flange to the top flange. While when the compression flange has an area more significant than the area of the tension flange, the values of C_b are smaller than their values for other locations of loads.
3. The changed slenderness of the beams has a significant impact on the moment gradient factor (C_b) as do the loading and end support conditions. The non-dimensional modified flexural-torsional slenderness of the beam λ_{LT} represents both the effect of span length and cross-section properties. Therefore, it offers a more exact understanding of the general variation of the factor of moment-gradient C_b .
4. A new formula for the modification factor (M_f) was introduced based on the sets of F.E.A. results to compute the value of the factor of moment-gradient C_b more accurately. This factor accurately expresses the lateral-torsional buckling capacity and helps estimate the required steel amount in design.

5.1. Recommendations For Future Work

1. Other forms and types of steel beams should be studied in future work, such as: (castellated beams, T-section, and C-sections).
2. Compare the outputs of numerical analysis with several other codes as well as the European code.

REFERENCES

- [1] S. Bas, "Web strain based prediction of web distortion influence on the elastic LTB limiting length," *Steel Composite Structures*, vol. 43, no. 2, pp. 271-278, 2022.DOI: <https://doi.org/10.12989/scs.2022.43.2.271>.
- [2] G. M. El-Mahdy, and M. M. El-Saadawy, "Ultimate strength of singly symmetrical I-section steel beams with variable flange ratio," *Thin-Walled Structures*, vol. 87, pp. 149-157, 2015/02/01/, 2015.DOI: <https://doi.org/10.1016/j.tws.2014.11.016>.
- [3] J. Kuś, "Lateral-torsional buckling steel beams with simultaneously tapered flanges and web," vol. 19, no. 4, pp. 897-916, 2015.DOI: <https://doi.org/10.12989/scs.2015.19.4.897>.
- [4] P. Code, "Eurocode 8: Design of structures for earthquake resistance-part 1: general rules, seismic actions and rules for buildings," Brussels: European Committee for Standardization, 2005.
- [5] A. K. Dessouki, A. B. AbdelRahim, and D. O. Abdul Hameed, "Bending strength of singly-symmetric overhanging floor I-beams," *HBRC Journal*, vol. 11, no. 2, pp. 176-193, 2015/08/01/, 2015.DOI: <https://doi.org/10.1016/j.hbrj.2014.03.003>.
- [6] J. M. Anderson, and N. S. J. J. o. t. s. d. Trahair, "Stability of monosymmetric beams and cantilevers," vol. 98, no. 1, pp. 269-286, 1972.DOI: <https://doi.org/10.1061/JSDEAG.0003114>.
- [7] S. Kitipornchai, and N. S. J. J. o. t. S. D. Trahair, "Buckling properties of monosymmetric I-beams," vol. 106, no. 5, pp. 941-957, 1980.DOI: <https://doi.org/10.1061/JSDEAG.0005441>.
- [8] A. W. Lamb, and C. D. J. J. o. S. E. Eamon, "Load height and moment factors for doubly symmetric wide flange beams," vol. 141, no. 12, pp. 04015069, 2015.DOI: [https://doi.org/10.1061/\(ASCE\)ST.1943-541X.0001332](https://doi.org/10.1061/(ASCE)ST.1943-541X.0001332).
- [9] N. S. Trahair, "Torsion Equations for Lateral Buckling (No. R964)," 2016.
- [10] S. Kitipornchai, C. M. Wang, and N. S. J. J. o. S. E. Trahair, "Buckling of monosymmetric I-beams under moment gradient," vol. 112, no. 4, pp. 781-799, 1986.DOI: [https://doi.org/10.1061/\(ASCE\)0733-9445\(1986\)112:4\(781\)](https://doi.org/10.1061/(ASCE)0733-9445(1986)112:4(781)).
- [11] S. Kitipornchai, and C. M. Wang, "Lateral buckling of tee beams under moment gradient," *Computers & Structures*, vol. 23, no. 1, pp. 69-76, 1986/01/01/, 1986.DOI: [https://doi.org/10.1016/0045-7949\(86\)90108-2](https://doi.org/10.1016/0045-7949(86)90108-2).
- [12] W.-b. Yuan, B. Kim, and C.-y. J. J. o. C. S. R. Chen, "Lateral-torsional buckling of steel web tapered tee-section cantilevers," vol. 87, pp. 31-37, 2013.DOI: <https://doi.org/10.1016/j.jcsr.2013.03.026>.
- [13] N.-H. Lim, N.-H. Park, Y.-J. Kang et al., "Elastic buckling of I-beams under linear moment gradient," vol. 40, no. 21, pp. 5635-5647, 2003.DOI: [https://doi.org/10.1016/S0020-7683\(03\)00330-5](https://doi.org/10.1016/S0020-7683(03)00330-5).
- [14] M. A. Serna, A. López, I. Puente et al., "Equivalent uniform moment factors for lateral-torsional buckling of steel members," vol. 62, no. 6, pp. 566-580, 2006.DOI: <https://doi.org/10.1016/j.jcsr.2005.09.001>.
- [15] T. A. Helwig, K. H. Frank, and J. A. J. J. o. S. E. Yura, "Lateral-torsional buckling of singly symmetric I-beams," vol. 123, no. 9, pp. 1172-1179, 1997.DOI: [https://doi.org/10.1061/\(ASCE\)0733-9445\(1997\)123:9\(1172\)](https://doi.org/10.1061/(ASCE)0733-9445(1997)123:9(1172)).
- [16] N.-H. Park, Y.-J. Kang, Y.-M. Jo et al., "Modification of C-equation in the SSRC Guide for buckling of monosymmetric I-beams under transverse loads," vol. 29, no. 12, pp. 3293-3300, 2007.DOI: <https://doi.org/10.1016/j.engstruct.2007.09.010>.
- [17] D. Bresser, G. J. P. Ravenshorst, and P. C. J. Hoogenboom, "General formulation of equivalent moment factor for elastic lateral torsional buckling of slender rectangular sections and I-sections,"

- Engineering Structures, vol. 207, pp. 110230, 2020/03/15/, 2020.DOI: <https://doi.org/10.1016/j.engstruct.2020.110230>.
- [18] R. Aydin, A. Gunaydin, N. Kirac et al., "On the evaluation of critical lateral buckling loads of prismatic steel beams," vol. 18, no. 3, pp. 603-621, 2015.DOI: <https://doi.org/10.4203/ccp.102.5>.
- [19] AISC 360-16, Specifications for Structural Steel Buildings, American Institute of Steel Construction; Chicago, USA, 2016., 2016.
- [20] C.-C. S16-14, Canadian Institute of Steel Construction, Handbook Of Steel Construction, CSA-S16-14 specification, Canada, Standards Council of Canada, 2014., 2014.
- [21] B. Yang, S.-B. Kang, G. Xiong et al., "Experimental and numerical study on lateral-torsional buckling of singly symmetric Q460GJ steel I-shaped beams," Thin-Walled Structures, vol. 113, pp. 205-216, 2017/04/01/, 2017.DOI: <https://doi.org/10.1016/j.tws.2016.12.009>.
- [22] A. S. Surla, and J. S. J. I. J. o. S. S. Park, "Experimental and numerical investigation on LTB strengths of monosymmetric compact I-beams with thickness-stepped-flanges," vol. 15, no. 4, pp. 933-944, 2015.DOI: <https://doi.org/10.1007/s13296-015-1214-6>.
- [23] A. J. P. ABAQUS, RI, USA, "Analysis User's Manual-version 6.13, Dassault Systemes Simulia Corp," 2013.
- [24] M. A. Bradford, and X. Liu, "Flexural-torsional buckling of high-strength steel beams," Journal of Constructional Steel Research, vol. 124, pp. 122-131, 2016/09/01/, 2016.DOI: <https://doi.org/10.1016/j.jcsr.2016.05.009>.
- [25] B. Yang, S. Nie, G. Xiong et al., "Residual stresses in welded I-shaped sections fabricated from Q460GJ structural steel plates," Journal of Constructional Steel Research, vol. 122, pp. 261-273, 2016/07/01/, 2016.DOI: <https://doi.org/10.1016/j.jcsr.2016.03.029>.
- [26] B. Selcuk, "Lateral torsional buckling of steel I-beams: Effect of initial geometric imperfection," Steel and Composite Structures, An International Journal, vol. 30, no. 5, pp. 483-492, 2019.DOI: <https://doi.org/10.12989/scs.2019.30.5.483>.

APPENDIX A

Design examples of the proposed equations:

Example 1:

Determine the critical moment for a steel beam in Figure (1) having the span of 5.0 m and the cross-section consisting of flange plates of 255.8 x 39.2 and a web plate of 614.5 x 14.5. The mechanical and material properties of the cross-section considered in the analysis are listed in Tables 1 and 2, respectively.

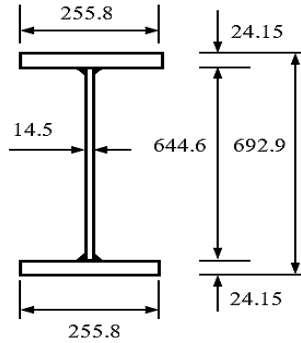


Figure A-1: Cross-section of the analyzed beam.

Table A-1. The mechanical properties of the I-section are applied in the numerical analysis.

Property	A cm ²	I _y cm ⁴	I _z cm ⁶	I _w dm ⁶	IT cm ⁴	Wpl.y cm ³
Value	217	170326	6630	7.42	308	5631

Table A-2. The material properties of the I-section are applied in the numerical analysis.

Property	Elastic modulus E (kN/mm ²)	Shear modulus G (kN/mm ²)	Uniaxial yield strength (MPa)	Plastic moment M _p (kN.m)
Value	210	81	265	1492

$$W = \frac{\pi}{L_b} \sqrt{\frac{EC_w}{G}}$$

$$W = \frac{\pi}{5000} \sqrt{\frac{210 \times 10^3 \times 7.42 \times 10^{12}}{81 \times 10^3 \times 308 \times 10^4}} = 1.57$$

$$M_{ocr} = \frac{\pi}{L_b} \sqrt{EI_y G J} \sqrt{1 + W^2}$$

$$M_{ocr} = \frac{\pi}{5000} \times$$

$$\sqrt{21 \times 10^4 \times 663 \times 10^5 \times 81 \times 10^3 \times 308 \times 1}$$

$$\sqrt{1 + 1.57^2}$$

$$M_{ocr} = 2.18 \times 10^9 \text{ N. mm} = 2180 \text{ kN. m}$$

$$\lambda_{LT} = \sqrt{\frac{M_p}{M_{ocr}}} = \sqrt{\frac{1492}{2180}} = 0.827$$

For constant bending moments along the segment and $\beta_f = 1.0$

$$a = 0.0$$

$$b = 0.016\beta_f^4 - 0.11\beta_f^3 + 0.30\beta_f^2 - 0.39\beta_f + 0.19$$

$$= 0.016 \times 1^4 - 0.11 \times 1^3 + 0.30 \times 1^2 - 0.39 \times 1 + 0.19 = 0.006$$

$$c = 0.02\beta_f^4 - 0.04\beta_f^3 + 0.13\beta_f^2 - 0.28\beta_f + 0.18$$

$$= 0.02 \times 1^4 - 0.04 \times 1^3 + 0.13 \times 1^2 - 0.28 \times 1 + 0.18 = 0.01$$

$$d = 1.59\beta_f^4 - 7.66\beta_f^3 + 11.57\beta_f^2 - 5.43\beta_f + 0.88$$

$$= 1.59 \times 1^4 - 7.66 \times 1^3 + 11.57 \times 1^2 - 5.43 \times 1 + 0.88 = 0.95$$

$$M_f = a \lambda_{LT}^3 + b \lambda_{LT}^2 + c \lambda_{LT} + d$$

$$= 0.0 + 0.006 \times 0.827^2 + 0.01 \times 0.827 + 0.95 = 0.96$$

$$\therefore \bar{C}_b = M_f \times C_{b(\text{code})} = 0.96 \times 1 = 0.96$$

$$M_{cr} = \bar{C}_b \times M_{ocr} = 0.96 \times 2180 = 2090 \text{ kN. m}$$

Example 2:

Determine the critical moment for a steel beam in Figure (2), having a span of 5.0 m and its cross-section consisting of the upper flange of 255.8 x 24.15, lower flange of 383.7 x 24.5, and web of 644.6 x 14.5. The mechanical and material properties of the cross-section considered in the analysis are listed in Tables 3 and 4, respectively.

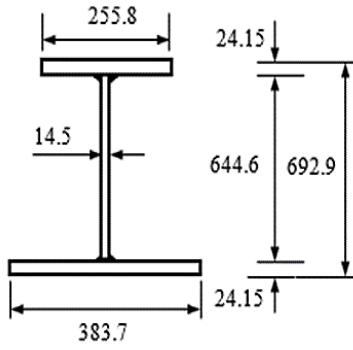


Figure A-2: Cross-section of the analyzed beam.

Table A-3: The mechanical properties of the I-section are applied in the numerical analysis.

Property	A cm ²	I _y cm ⁴	I _z cm ⁶	I _w dm ⁶	IT cm ⁴	Wpl. y cm ³
Value	248	200809	14754	11.621	365.75	6506

Table A-4. The material properties of the I-section are applied in the numerical analysis.

Property	Elastic modulus E (kN/mm ²)	Shear modulus G (kN/mm ²)	Uniaxial yield strength (MPa)	Plastic moment M _p (kN.m)
Value	210	81	265	1724

$$W = \frac{\pi}{L_b} \sqrt{\frac{EC_w}{GJ}}$$

$$W = \frac{\pi}{5000} \sqrt{\frac{210 \times 10^3 \times 11.621 \times 10^{12}}{81 \times 10^3 \times 365.75 \times 10^4}} = 1.8$$

$$M_{ocr} = \frac{\pi}{L_b} \sqrt{EI_y GJ} \sqrt{1 + W^2}$$

$$M_{ocr} = \frac{\pi}{5000}$$

$$\sqrt{21 \times 10^4 \times 14754 \times 10^4 \times 81 \times 10^3 \times 365.75 \times 10^4}$$

$$\sqrt{1 + 1.8^2}$$

$$M_{ocr} = 3.92 \times 10^9 \text{ N.mm} = 3920 \text{ kN.m}$$

$$\lambda_{LT} = \sqrt{\frac{M_p}{M_{ocr}}} = \sqrt{\frac{1724}{3920}} = 0.663$$

For constant bending moments along the segment and $\beta_f = 0.67$

$$a = 0.0$$

$$b = 0.016\beta_f^4 - 0.11\beta_f^3 + 0.30\beta_f^2 - 0.39\beta_f + 0.19$$

$$= 0.016 \times 0.67^4 - 0.11 \times 0.67^3 + 0.30 \times 0.67^2 - 0.39 \times 0.67 + 0.19 = 0.034$$

$$c = 0.02\beta_f^4 - 0.04\beta_f^3 + 0.13\beta_f^2 - 0.28\beta_f + 0.18$$

$$= 0.02 \times 0.67^4 - 0.04 \times 0.67^3 + 0.13 \times 0.67^2 - 0.28 \times 0.67 + 0.18 = 0.04$$

$$d = 1.59\beta_f^4 - 7.66\beta_f^3 + 11.57\beta_f^2 - 5.43\beta_f + 0.88$$

$$= 1.59 \times 0.67^4 - 7.66 \times 0.67^3 + 11.57 \times 0.67^2 - 5.43 \times 0.67 + 0.88$$

$$M_f = a \lambda_{LT}^3 + b \lambda_{LT}^2 + c \lambda_{LT} + d$$

$$= 0.0 + 0.034 \times 0.663^2 + 0.04 \times 0.827 + 0.45 = 0.49$$

$$\therefore \bar{C}_b = M_f \times C_{b(\text{code})} = 0.49 \times 1 = 0.49$$

$$M_{cr} = \bar{C}_b \times M_{ocr} = 0.49 \times 3920 = 1921 \text{ kN.m}$$